HHS Public Access

Author manuscript

*Biomarkers*. Author manuscript; available in PMC 2018 June 05.

Published in final edited form as:

*Biomarkers*. 2018 March ; 23(2): 154–160. doi:10.1080/1354750X.2017.1380082.

# Quantification of manganese and mercury in toenail *in vivo* using portable X-ray fluorescence (XRF)

**Xinxin Zhang**[a,#], **Aaron J. Specht**[b], **Marc G. Weisskopf**[b], **Jennifer Weuve**[c], and **Linda H. Nie**[a]

[a]School of Health Sciences, Purdue University, West Lafayette, IN, USA

[b]Department of Environmental Health, Harvard T.H. Chan School of Public Health, Boston, MA, USA

[c]Department of Epidemiology, Boston University School of Public Health, Boston, MA, USA

## Abstract

**Background and objective—**Toenail is an advantageous biomarker to assess exposure to metals such as manganese and mercury. Toenail Mn and Hg are in general analyzed by chemical methods such as inductively coupled plasma mass spectrometry and atomic absorption spectrophotometry. In this project, a practical and convenient technology—portable X-ray florescence (XRF)—is studied for the noninvasive *in vivo* quantification of manganese and mercury in toenail.

**Material and methods—**The portable XRF method has advantages in that it does not require toenail clipping and it can be done in 3 min, which will greatly benefit human studies involving the assessment of manganese and mercury exposures. This study mainly focused on the methodology development and validation which includes spectral analysis, system calibration, the effect of toenail thickness, and the detection limit of the system. Manganese- and mercury-doped toenail phantoms were made. Calibration lines were established for these measurements.

**Results—**The results show that the detection limit for manganese is 3.65 μg/g (ppm) and for mercury is 0.55 μg/g (ppm) using 1 mm thick nail phantoms with 10 mm soft tissue underneath.

**Discussion and conclusion—**We conclude that portable XRF is a valuable and sensitive technology to quantify toenail manganese and mercury *in vivo*.

### Keywords

Heavy metal; *in vivo*; Mn and Hg exposure assessment; portable XRF; toenail

CONTACT Linda H. Nie, hnie@purdue.edu, School of Health Sciences, Purdue University, 550 Stadium Mall Drive, West Lafayette, IN 47906, USA.

[#]Xinxin Zhang is responsible for statistical design/analysis. zhan2378@purdue.edu

**ORCID**

Xinxin Zhang, http://orcid.org/0000-0003-3667-9302

**Disclosure statement**

No potential conflict of interest was reported by the authors.

## Introduction

Manganese (Mn) is an essential element, and its high-level exposure has been related to many chronic health effects especially to adverse neurological outcomes (Crossgrove and Zheng 2004, Jiang *et al.* 2006). Mn is a common metal that exists in food, water and soil. Moderate-to-high levels of Mn exposure have been reported among populations of workers occupationally exposed to Mn, such as ferromanganese welders (Wang *et al.* 1989) or steel smelting workers (Wennberg *et al.* 1991). Mn overexposure in the human body has been investigated over the last few decades (Rodier 1955, Crossgrove and Zheng 2004, Bowman *et al.* 2011). Brain is the most vulnerable target in relation to Mn accumulation. Mn-induced damage to the central nervous system can lead to chronic neurobehavial disorders resembling Parkinson's disease, which has been confirmed in many studies (Wang *et al.* 1989, Levy and Nassetta 2003, Jiang *et al.* 2006).

Mercury is a toxic heavy metal. Adverse health outcomes from Hg exposure to the general population have been a significant public health issue for many decades. The US Environmental Protection Agency (EPA) recently announced to reduce the reference dose (RfD) for methylmercury (MeHg) intake from 0.3 μg/kg/day to 0.1 μg/kg/day (US EPA 2011). Hg exposure comes from a variety of sources, e.g. inhaled mercury vapor from the environment or dental amalgam and methylmercury ($CH_3Hg^+$) by seafood consumption. Inorganic mercury and MeHg are the two chemical forms of Hg that accumulate in the human body after exposure, each with different metabolisms and clinical toxicological features. Generally speaking, most inorganic mercury can be rapidly excreted from the human body through urine. However, as a common element from consuming seafood, MeHg is the more cumulative neurotoxicant targeting the human brain. Many Hg-associated chronic neurological disorders and human developmental issues have been reported, such as disability of fine motor skills and verbal memory (Agency for Toxic Substances and Disease Registry 1999; Staff 2000).

Previous studies have evaluated the use of toenails as a biomarker of Mn and Hg exposure with promising results. Compared to the short half-life of Mn and Hg in other traditional biomarkers such as blood and urine, toenail is an advantageous cumulative biomarker which typically reflects exposures in a relatively longer period, e.g. Mn exposures over 7–12 months (Laohaudomchok *et al.* 2011). In addition, total-Hg concentrations in toenails is significantly correlated to the concentrations of MeHg in blood and occipital lobe cortex (Bjorkman *et al.* 2007), therefore, it is a good indicator of MeHg exposure. Furthermore, toenail is generally less contaminated compared to hair and fingernail.

The goal of our current work is to explore a practical and convenient portable X-ray fluorescence (XRF) technology to quantify the concentrations of Mn and Hg in toenail *in vivo*. The portable XRF technology was developed and validated in our group, and was successfully used to noninvasively quantify the bone lead concentration *in vivo* within 3 min (Nie *et al.* 2011, Specht *et al.* 2014, 2016). Furthermore, portable XRF applications in different metal assessment in human nail and nail clippings have been widely investigated in recent studies (Gherase and Fleming 2011, McIver *et al.* 2015, Fleming and Ware 2017).

The current project investigated a calibration method of the potable XRF device to quantify Mn and Hg concentration in human toenail *in vivo*.

The portable XRF technique has benefits over the standard inductively coupled plasma mass spectrometry (ICP-MS) approach, since it requires no collection of toenail clippings and can be processed within a short period of time in a more cost-effective way. Additionally, this technique overcomes the poor sensitivity of atomic absorption spectrophotometry (AAS) method for Hg exposure assessment due to its extreme volatility. To develop this novel technology, the system design was optimized to obtain a lower detection limit for Mn and Hg, contributing a better measurements precision *in vivo* at lower metal concentration. Furthermore, simultaneous assessment of Mn and Hg can be performed with the portable XRF device.

## Clinical significance

- Moderate-to-high-level exposure to manganese (Mn) and low-to-high-level exposure to mercury (Hg) are associated with adverse health effects, especially neurological disorders.
- *In vivo* portable X-ray fluorescence (XRF) is a convenient and fast way to assess manganese and mercury exposures.
- The portable XRF technology has been calibrated to quantify Mn and Hg concentrations in human toenail *in vivo*.
- The sensitivity of the system allows for simultaneous exposure assessment of both metals.

## Material and method

### Portable XRF device

A customized portable XRF device with improved technology in geometry and detector was used in this project (XL3t GOLDD+, Thermo Fisher Scientific Inc., Billerica, MA). The portable XRF device has an energy span up to 50 keV and uses a thermoelectric-cooled silicon drift detector with 25 $mm^2$ area and 1 mm thickness. The X-ray tube settings were optimized for Mn and Hg measurements with a voltage of 40 kVp and a current of 50 μA. A variety of filter combinations with different thickness can be selected in this device. A silver (Ag) and iron (Fe) combination filter was selected in our study, which provides the best detection limit for the measurement of Mn and Hg in human nail. Figure 1 illustrates a schematic configuration of heavy metal assessment in nail with the portable XRF device. Our study focused on investigating the K-shell characteristic X-ray produced by the photoelectric interaction in toenail for Mn quantification and the L-shell characteristic X-ray for Hg concentration assessment. Those detected X-rays are further processed and digitized by employed electronics in the device.

## Nail phantom

A polyester resin–salt mixture substitute for nail phantom was selected in order to simulate the attenuation properties of human nail (Roy *et al.* 2010) at the relevant K-shell X-ray energy of 5.90 keV for Mn and L-shell energy of 9.99 keV for Hg. In Table 1, elemental composition, density and mass attenuation coefficient for resin, salt, nail phantom and human nail are listed. According to the table, by mixing a mass of 95% commercial polyester resin (Bondo Corp. Atlanta, GA) and 5% salt (Morton Salt Inc., Chicago, IL), human toenail can be successfully simulated.

Different concentrations of Mn and Hg were doped into the nail-equivalent phantoms with a range from 0 to 50 ppm (0, 5, 10, 15, 20, 30, 45 and 50 ppm). A manganese (II) nitrate solution (Flinn Scientific Inc., Batavia, IL) with a concentration of 0.24 g/mL was used for the Mn phantoms. The mercury solution was an atomic absorption spectrometry standard (Fisher scientific company LLC, Bridgewater, NJ) with a concentration of 1 mg/mL. After looking up the range of nail thickness found by Johnson and Shuster (1994), nail phantoms with 1.0 and 3.0 mm thickness were formed by pouring well-mixed resin into a plastic rectangular shape mold of 2.2 × 2.4 cm. Furthermore, Lucite plates were used to simulate the soft tissue underneath toenails. To study how the soft tissue thickness under the nail will affect the system calibration and data analysis, measurements were made for 0 and 50 ppm phantoms with 14 different thicknesses of Lucite (from 0 to 14.56 mm) placed under the phantom. Background counts under the Mn X-ray peaks for the 0 ppm phantom were plotted against Lucite thickness. The net Mn X-ray counts for the 50 ppm phantom versus Lucite thickness was also plotted. One centimeter Lucite was used as soft tissue backing under the nail.

## Spectrum analysis

Multiple-peak fitting was conducted for spectral analysis. The Mn $K_\alpha$ peak region was fitted over a range from 5.7 to 6.2 keV. A noticeable Fe $K_\alpha$ peak generated from surrounding shielding of the portable XRF device is found in the spectrum with energy of 6.4 keV. This coupled Fe peak significantly interferes with the peak of interest. In addition, the Hg $L_{\alpha 1}$ peak found at 9.99 keV is at the right edge of and slightly overlapping with the $L_{\beta 1}$ peak of tungsten (W), which is the main composition of the collimator and tube base in the portable XRF device itself. Mn and Hg spectrum were analyzed independently, with our multiple-peak fitting technique using the same function as listed in Equation (1) and a least-squares algorithm. Peak of interest and peak of interference were fitted simultaneously with the same Gaussian distribution for each to represent the net X-ray count. A scattering peak in the Mn spectrum and a W Compton peak in the Hg spectrum was fitted with the third Gaussian function. A constant was used to describe the background.

$$f(x) = A_0 e^{-\frac{(x-B_0)^2}{2\sigma_{Mn/Hg}^2}} + A_1 e^{-\frac{(x-B_1)^2}{2\sigma_{Fe/W}^2}} + A_2 e^{-\frac{(x-B_2)^2}{2\sigma^2}} + A_3 \quad (1)$$

where $A_0$, $A_1$ and $A_2$ represent the amplitude of peak, $B_0$, $B_1$ and $B_2$ are the positions of the peaks, and $\sigma_{Mn=Hg}$, $\sigma_{Fe=W}$ and $\sigma$ are the variances. $A_3$ is the background.

### Radiation dose assessed with TLDs

In order to estimate the dose of the system at the skin surface, four thermoluminescent dosimeters chips (TLDs) with diameter of 0.5 cm were placed at the window surface of the portable XRF device, which covers ~1 $cm^2$ area. A 3 mm blank nail phantom was placed on the top of TLD chips. After measuring the phantom for 3 min, the TLDs were read out by a TLD reader equipment (Harshaw TLD 4000; Harshaw Partnership, Solon, OH, USA).

## Results

### Spectrum fitting for Mn and Hg

As described in the Material and method section, Fe in surrounding shielding of the device generates an Fe $K_\alpha$ peak which is located adjacent to the Mn $K_\alpha$ peak. Figure 2 shows an example of the Mn spectrum and its fitted curve, where a 1-mm 50-ppm Mn-doped toenail phantom was measured for 3 min. As shown in the figure, there is a significant amount of Fe contributing to the background counts in the Mn region, particularly, interfering the net count determination for relatively lower Mn concentrations. Furthermore, a scattering peak was found in the region ~6.2 keV, which also interferes with the Mn peak. Using the multi-peak fitting and least-square algorithm, the obtained $\chi^2$ of fitted spectra for all phantoms range from 0.89 to 1.40.

The multiple-peak fitting algorithm was also applied in the Hg spectrum analysis, as the W $L_{\beta 1}$ peak with energy of 9.67 keV and relative density of 67% is overlapping with the Hg $L_{\alpha 1}$ peak. Figure 3(a) shows the fitted curve in the spectrum measured with a 1 mm of 50 ppm Hg-doped toenail phantom. As shown in the figure, a W Compton peak interferes with the W $L_{\beta 1}$ peak, and hence a third Gaussian function was used to describe this peak. The fitted $\chi^2$ of all phantom measurements (0–50 ppm) ranged from 1.31 to 1.85.

AW $L_{\beta 2}$ peak with energy of 9.96 keV and relative density of 21% is indistinguishable from the Hg $L_{\alpha 1}$ peak. This peak is noticeable with 0 ppm Hg-doped phantom showed in Figure 3(b). As mentioned earlier, W comes from the portable XRF device itself. Therefore, the W peaks are expected to be consistent with the same setting among the phantoms. Hence, the interference of the W $L_{\beta 2}$ peak can be extracted from the intercept of calibration line without being added to the spectral fitting.

### Lucite/soft tissue thickness

Figure 4 shows the total background counts under the Mn $K_\alpha$ peak for the 0 ppm phantom versus Lucite thickness. The background increased with the increase of soft tissue and then flattened at ~10 mm. This is expected because the scattering increases with the increase of the soft tissue thickness, and saturates at certain thickness. Figure 5 shows the net counts of 50 ppm Mn-doped phantoms versus Lucite thickness. The $p$ value of the fitted linear regression curve was 0.63, which indicates that the obtained slope was not significantly

different from zero at a 5% level, and that the net count of the Mn peak is not associated with the soft tissue thickness underneath the toenail.

### Calibration line of toenail Mn and Hg

Based on the developed method of spectrum analysis described in the previous sections, calibration lines are created using Mn- and Hg-doped nail phantoms. The calibration lines established by 1- and 3-mm Mn-doped phantoms are shown in Figure 6(a), and the obtained $R^2$ were 0.995 and 0.993, respectively. A calibration line was also made for 1-mm toenail phantoms with 10 mm of Lucite placed underneath to simulate the *in vivo* situation (Figure 6(b)). The $R^2$ of this calibration line was 0.989.

The calibration lines of 1- and 3-mm Hg-doped phantoms associated with $L_{\alpha 1}$ peak are shown in Figure 7(a), while the calibration line of the 1-mm phantom with 10-mm Lucite is shown in Figure 7(b). The $R^2$ obtained were 0.985, 0.994 and 0.988, respectively. The concentration of the indistinguishable W $L_{\beta 2}$ peak is associated with the intercept (parameter *a* in figures) of the established calibration line, which needs to be extracted to quantify the Hg concentration *in vivo* with the portable XRF.

The toenail Mn and Hg concentrations for *in vivo* measurements can be calculated from the *in vivo* spectra and the calibration lines shown in Figures 6(b) and 7(b).

### Detection limit of the portable XRF device

The Mn- and Hg-doped 1-mm toenail phantoms with 10-mm Lucite were used for the calculation of detection limit of the system. The detection limit was calculated as in Equation (2).

$$DL = 2 * \sigma_{0ppm} = 2 * \frac{\sqrt{BKG_0}}{slope} \quad (2)$$

Where, $BKG_0$ is the background count within 3 min under the $K_\alpha$ or $L_{\alpha 1}$ peak for the 0-ppm phantoms, *slope* is the slope of the calibration line illustrated in the previous section. Table 2 shows the results of detection limit in μg/g for both Mn at the $K_\alpha$ region and Hg at the $L_{\alpha 1}$ region.

### Dose of the portable XRF device

With the TLD chips, the average entrance dose to the 1 $cm^2$ nail area was measured to be 43 mSv, and the dose to the tissue under the nail is expected to be smaller. To be conservative, entrance dose was assumed to be a skin entrance dose. Skin surface area for a reference man is 1.9 $m^2$ (Verbraecken *et al.* 2006), and a total body bone area is 0.23 $m^2$ (Looker *et al.* 2013), hence, the whole body effective dose was estimated to be 0.21 μSv with conservative calculation. In the previous study for bone lead (Pb) (Specht *et al.* 2014), entrance dose was obtained as 31 mSv. The skin entrance dose is comparable in these two studies, given that slightly different X-ray tube settings and a different number of TLDs were used. As the shallow dose is defined as the dose averaged over a 10 $cm^2$ area of skin, a 43 mSv entrance

skin dose to 1 $cm^2$ skin is ~1% of the allowable yearly occupational extremity dose limit of 500 mSv. The risk of exposure to 0.21 μSv of radiation is negligible comparing to the annual background radiation dose of 3.6 mSv for general population in USA.

## Discussion

The current study investigated the feasibility of quantifying Mn and Hg in toenail *in vivo* using portable XRF technology. The investigation mainly focused on the methodology of spectral analysis, system calibration, effect of toenail thickness on results, detection limit, and the associated radiation dose to a human subject. Compared to the method of assessing metal concentrations in bone, XRF toenail metal measurements do not have the issue of soft tissue attenuation because the target is toenail, which is unencumbered by overlying tissues.

The impact on signal collection from toenail thickness was investigated in our study. As shown in our results, the net counts of the peak of interest are close to equivalent in the 1 and 3 mm toenail phantoms. This is due to the high photon attenuation associated with the characteristic X-rays generated in the two different thickness phantoms. Using theoretical calculations, more than 95% of the Mn $K_\alpha$ X-ray will be attenuated in 1 and 3 mm toenail phantoms; and the attenuation of Hg $L_\alpha$ X-ray in 1–3 mm toenail phantoms ranges from 50 to 87%. Even though the number of characteristic X-rays produced inside the phantom should increase with thicker phantoms, only a small quantity of net counts are detectable due to such increasing self-absorption in the sample. Thus, the calibration for *in vivo* measurements does not change significantly over different toenail thicknesses. According to Johnson and Shuster (1994), human's great toe-nail thickness ranges from 0.83 to 1.69 mm. Hence, 1-mm phantom with 10-mm Lucite was selected for methodology exploration and system calibration. Even though the tissue under nail was not directly related to photon attenuation, it affects the background under the interested X-ray peaks due to the increase of Compton scattering with the increase of the soft tissue. As a consequence, the increased soft tissue led to a worse detection limit of the system, until the saturation of the scattering is reached.

The detection limit of the portable XRF system for Hg exposure assessment *in vivo* was achieved as 0.55 μg/g (ppm), which was comparable to the toenail Hg level found in general population by Ohno et al. (2007) and by Alfthan (1997). With such this sensitivity, we conclude that *in vivo* quantification of Hg with the portable XRF is feasible. Standard approaches for toenail metal exposure analysis, such as ICP-MS, AAS or CVAS (cold vapor atomic fluorescence spectroscopy), require nail clippings and the analysis procedure can be very time consuming. More importantly, the volatility of Hg can result in a more sophisticated preparation method for some of the approaches. In contrast, the portable XRF technique provides a quick 3-min measurement, which helps avoid the difficulties in collecting toenail clippings, and allows for the analysis of data in a more cost-effective way.

The detection limit for toenail Mn quantification was 3.65 μg/g with 10 mm of Lucite and 1-mm toenail phantoms. Even though the sensitivity of Mn is not as good as Hg in low-level exposure, the portable XRF can still can be considered as a competitive technique for high-

exposure population, which is supported by the fact that a weighted mean of 4.22 ppm nail Mn was found in the general population by Slotnick *et al.* (2005).

The detection limit for the system could be improved further using different device specifications specifically optimized for the measurements, including selection of filter combination, X-ray tube settings, and fitting algorithm. Note that in the Mn spectrum analysis, a higher uncertainty of the Mn net count was obtained due to the simultaneous peak fitting for both Mn and Fe. Furthermore, a scattering peak was found in the region ~6.2 keV. Even though a Gaussian function was adopted to fit this scattering peak, the origins of this peak remain unclear and proper identification of the peak would lead to a more precise fitting procedure.

In future work, the portable XRF system will be validated by measuring Mn and Hg concentration in toenail *in vivo* in a population study, and comparing these results with Mn and Hg concentrations obtained from collected toenails analyzed by standard ICP-MS and/or neutron activation analysis (NAA).

## Conclusion

The current study explored the use of portable XRF technology for the assessment of Mn and Hg in toenail *in vivo*. The detection limit of the device for toenail Mn and Hg were calculated to be 3.65 and 0.55 μg/g, respectively. The detection limit for the system could be improved further using different device specifications specifically optimized for the measurements. Future study will investigate the quantification of Mn and Hg with the portable XRF in toenail *in vivo* in a human population, and the results will be compared with standard approaches.

## Acknowledgments

The authors would like to thank the radiological and environmental management (REM) department at Purdue University for the support on the radiation dosimetry study.

**Funding**

The research described in this article was supported by National Institute of Environmental Health Sciences (NIH/NIEHS-1R21 ES024700).

## References

Alfthan GV. Toenail mercury concentration as a biomarker of methylmercury exposure. Biomarkers: Biochemical indicators of exposure, response, and susceptibility to chemicals. 1997; 2:233–238.

Bjorkman L, et al. Mercury in human brain, blood, muscle and toenails in relation to exposure: an autopsy study. Environmental health. 2007; 6:30. [PubMed: 17931423]

Bowman AB, et al. Role of manganese in neurodegenerative diseases. Journal of trace elements in medicine and biology: organ of the society for minerals and trace elements (GMS). 2011; 25:191–203.

Crossgrove J, Zheng W. Manganese toxicity upon overexposure. NMR in biomedicine. 2004; 17:544–553. [PubMed: 15617053]

Fleming DE, Ware CS. Portable x-ray fluorescence for the analysis of chromium in nail and nail clippings. Applied radiation and isotopes: including data, instrumentation and methods for use in agriculture, industry and medicine. 2017; 121:91–95.

Gherase MR, Fleming DE. A calibration method for proposed XRF measurements of arsenic and selenium in nail clippings. Physics in medicine and biology. 2011; 56:N215–N225. [PubMed: 21937772]

Jiang YM, et al. Effective treatment of manganese-induced occupational Parkinsonism with p-aminosalicylic acid: a case of 17-year follow-up study. Journal of occupational and environmental medicine. 2006; 48:644–649. [PubMed: 16766929]

Johnson M, Shuster S. Determinants of nail thickness and length. The British journal of dermatology. 1994; 130:195–198. [PubMed: 8123571]

Laohaudomchok W, et al. Toenail, blood, and urine as biomarkers of manganese exposure. Journal of occupational and environmental medicine. 2011; 53:506–510. [PubMed: 21494156]

Levy BS, Nassetta WJ. Neurologic effects of manganese in humans: a review. International journal of occupational and environmental health. 2003; 9:153–163. [PubMed: 12848244]

Looker AC, et al. Total body bone area, bone mineral content, and bone mineral density for individuals aged 8 years and over: United States, 1999–2006. Vital health and statistics. 2013; 11:1–78.

Mciver DJ, et al. Evaluation of a novel portable x-ray fluorescence screening tool for detection of arsenic exposure. Physiological measurement. 2015; 36:2443–2459. [PubMed: 26536141]

Nie LH, et al. *In vivo* quantification of lead in bone with a portable x-ray fluorescence system-methodology and feasibility. Physics in medicine and biology. 2011; 56:N39–N51. [PubMed: 21242629]

Ohno T, et al. Total mercury levels in hair, toenail, and urine among women free from occupational exposure and their relations to renal tubular function. Environmental research. 2007; 103:191–197. [PubMed: 16890218]

Rodier J. Manganese poisoning in Moroccan miners. British journal of industrial medicine. 1955; 12:21–35. [PubMed: 14351643]

Roy CW, Gherase MR, Fleming DE. Simultaneous assessment of arsenic and selenium in human nail phantoms using a portable x-ray tube and a detector. Physics in medicine and biology. 2010; 55:N151–N159. [PubMed: 20182007]

Slotnick MJ, et al. Profiles of trace elements in toenails of Arab-Americans in the Detroit area, Michigan. Biological trace element research. 2005; 107:113–126. [PubMed: 16217136]

Specht AJ, et al. XRF-measured bone lead (Pb) as a biomarker for Pb exposure and toxicity among children diagnosed with Pb poisoning. Biomarkers: biochemical indicators of exposure, response, and susceptibility to chemicals. 2016; 21:347–352.

Specht AJ, Weisskopf M, Nie LH. Portable XRF technology to quantify Pb in bone *in vivo*. Journal of biomarkers. 2014; 2014:398032. [PubMed: 26317033]

Staff, NRC. Toxicological effects of methylmercury. Washington: National Academies Press; 2000.

Agency for Toxic Substances and Disease Registry. Toxicological profile for mercury. Atlanta, GA: U.S. Dept. of Health and Human Services, Public Health Service, Agency for Toxic Substances and Disease Registry; 1999.

US Environmental Protection Agency. Methylmercury (MeHg) (CASRN 22967-92-6). Washington, DC: Integrated Risk Information System, U.S. Environmental Protection Agency; 2011.

Verbraecken J, et al. Body surface area in normal-weight, overweight, and obese adults. A comparison study. Metabolism: clinical and experimental. 2006; 55:515–524. [PubMed: 16546483]

Wang JD, et al. Manganese induced parkinsonism: an outbreak due to an unrepaired ventilation control system in a ferromanganese smelter. British Journal of Industrial Medicine. 1989; 46:856–859. [PubMed: 2611159]

Wennberg A, et al. Manganese exposure in steel smelters a health hazard to the nervous system. Scandinavian journal of work, environment & health. 1991; 17:255–262.

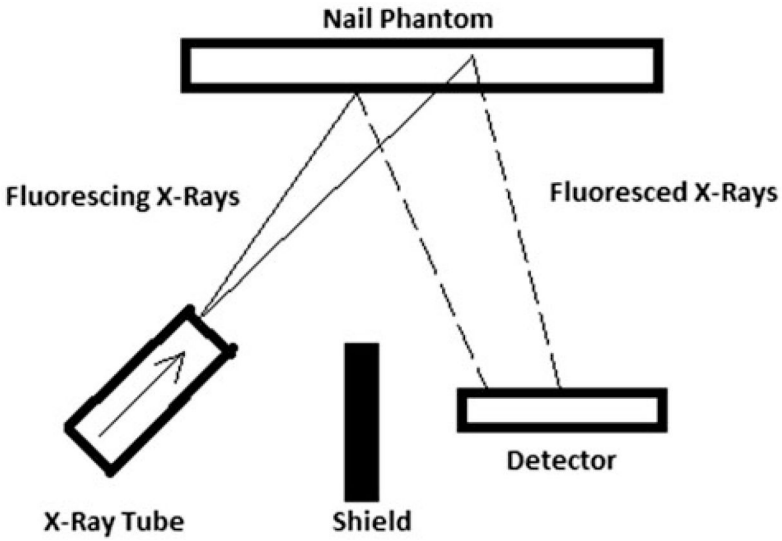


**Figure 1.**
Schematic configuration of portable XRF device in nail phantom measurement.

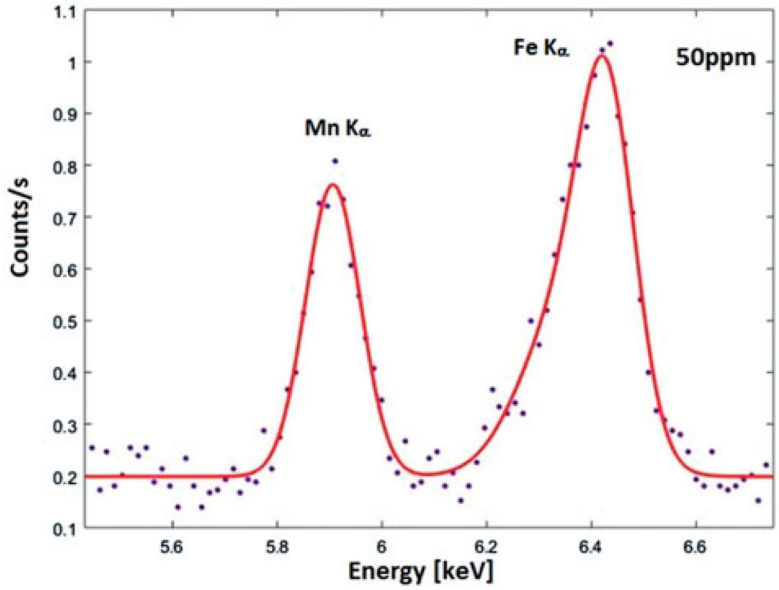


**Figure 2.**
Observed and fitted Mn $K_\alpha$ peak in company with Fe $K_\alpha$ peak for the 50 ppm Mn toenail phantom.

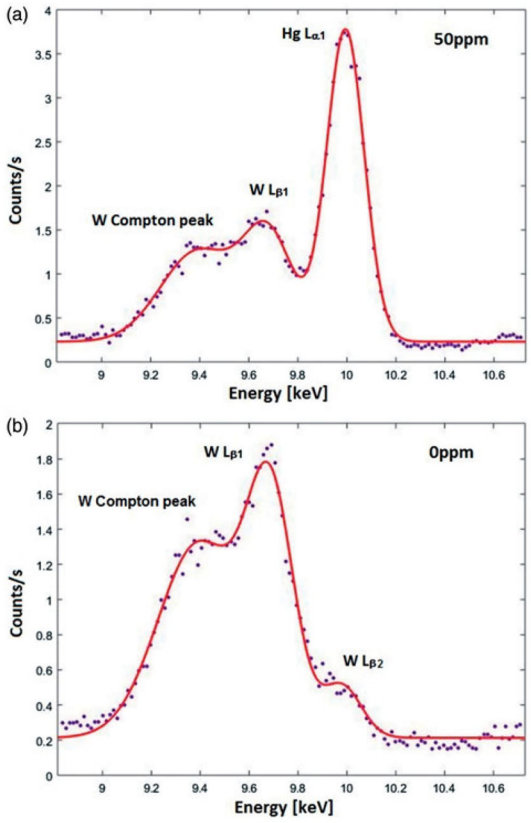


**Figure 3.**

(a) Observed and fitted Hg $L_{\alpha 1}$ peak in company with W $L_{\beta 1}$ peak and its Compton peak for the 50 ppm Hg toenail phantom. (b) Observed and fitted Hg $L_{\alpha 1}$ peak in company with W $L_{\beta 1}$ peak, its Compton peak and W $L_{\beta 2}$ peak for the 0 ppm Hg toenail phantom.

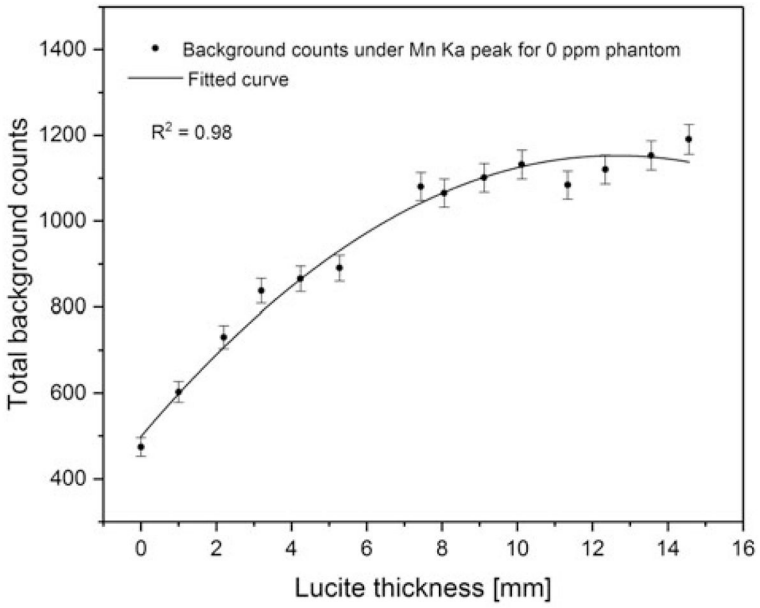


**Figure 4.**

Total background counts under Mn $K_\alpha$ peak for 0 ppm Mn-doped phantom versus Lucite thickness.

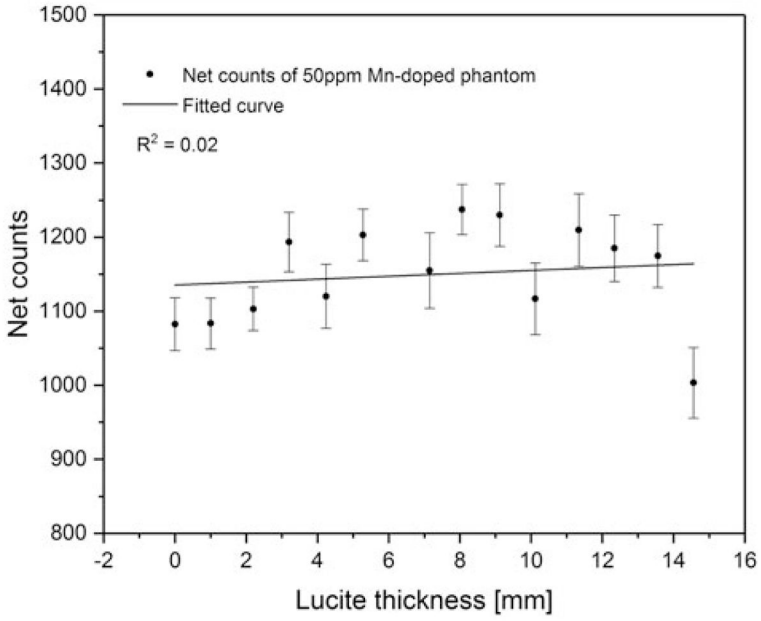


**Figure 5.**
Net counts of 50 ppm Mn-doped phantom versus Lucite thickness.

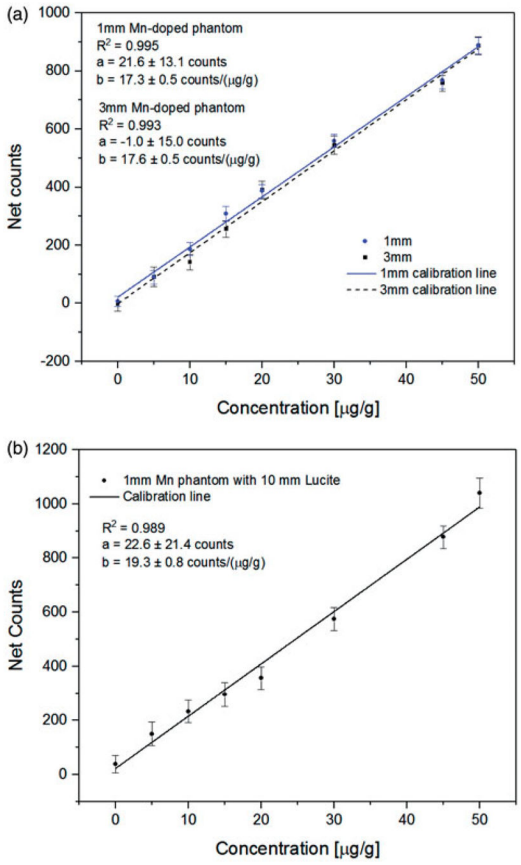


**Figure 6.**

(a) Calibration line of 1 and 3 mm Mn-doped phantoms with portable XRF. (b) Calibration line of 1 mm Mn-doped phantoms with 10 mm Lucite with portable XRF.

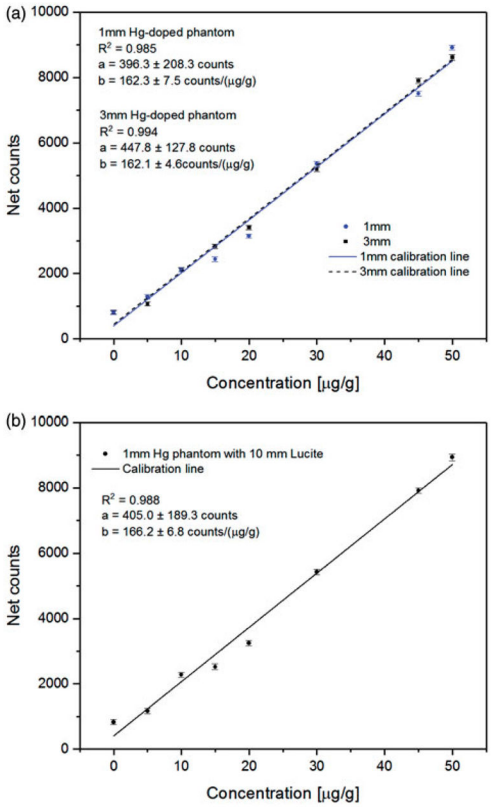


**Figure 7.**

(a) Calibration line of 1 and 3 mm Hg-doped phantoms measurements with portable XRF. (b) Calibration line of 1 mm Hg-doped phantoms with 10 mm Lucite measurements with portable XRF.

**Table 1**

Elemental composition, density, total mass attenuation coefficient and photoelectric absorption coefficient for resin, salt, nail phantom and human nail.

| | | | Total attenuation ($cm^2/g$) | | Photoelectric absorption ($cm^2/g$) |
|---|---|---|---|---|---|
| **Substance** | **Elemental composition (% mass)** | **dDensity ($g/cm^3$)** | **5.90 keV** | **9.99 keV** | **22 keV** |
| Resin | 5 H, 60 C, 35 O | 1.2 | 17.13 | 3.63 | 0.25 |
| Salt | 39 Na, 61 Cl | 2.2 | 181.1 | 42.2 | 3.85 |
| Nail phantom | 4.75 H, 57 C, 33.25 O, 1.97 Na, 3.05 Cl | 1.25 | 25.34 | 5.56 | 0.43 |
| Human nail | 7 H, 45 C, 15 N, 29 O, 4 S | 1.3 | 25.38 | 5.57 | 0.43 |

**Table 2**

Detection limit for 1 mm toenail Mn and Hg measurement by portable XRF with and without the soft tissue backing.

| | Mn $K_{\alpha}$ (μg/g) | Hg $L_{\alpha 1}$ (μg/g) |
|---|---|---|
| Bare phantom | 2.37 | 0.49 |
| Phantom with 10 mm Lucite backing | 3.65 | 0.55 |